

# Finite Nuclei in a Relativistic Mean-Field Model with Derivative Couplings

M. Chiapparini

*Departamento de Física Nuclear e Altas Energias*

*Centro Brasileiro de Pesquisas Físicas*

*Rua Xavier Sigaud 150, 22290-180 Rio de Janeiro RJ, Brazil*

A. Delfino, M. Malheiro\*

*Instituto de Física - Universidade Federal Fluminense*

*Outeiro de São João Batista s/n, 24020-004 Centro, Niterói*

*Rio de Janeiro, Brazil*

A. Gattone

*Departamento de Física. Comisión Nacional de Energía Atómica,*

*Av. del Libertador 8250, 1429 Buenos Aires, Argentina*

(November 19, 2018)

## Abstract

We study finite nuclei, at the mean-field level, using the Zimanyi-Moskowski model and one of its variations (the ZM3 model). We calculate energy levels and ground-state properties in nuclei where the mean-field approach

---

\*Present address: Department of Physics and Astronomy, University of Maryland, College Park, MD 20742, USA

is reliable. The role played by the spin-orbit potential in sorting out mean-field model descriptions is emphasized.

## I. INTRODUCTION

At the mean-field level the linear  $\sigma - \omega$  (or Walecka) model [1] satisfactorily explains many properties of nuclear matter and finite nuclei with two free parameters. The resulting nuclear-matter compression modulus at saturation density exceeds, however, the experimental bound [2,3]. A way out of this difficulty is to introduce non-linear scalar self-couplings [4,5]. The non-linear model that obtains has been shown to reproduce well ground-state nuclear properties (though with some instabilities at high densities and for low values of the compressibility,  $\kappa \lesssim 200$  MeV [5]). This model is renormalizable and has four free parameters to fit.

One alternative approach which renders a satisfactory compression modulus without increasing the number of free parameters is that advanced by Zimanyi and Moszkowski [6] and by Heide and Rudaz [7]. This model employs the same degrees of freedom and the same number of independent couplings that are present in the Walecka model. The difference lies in the coupling among the fields. In the work of Zimanyi and Moszkowski (ZM), for instance, the authors use a non-renormalizable derivative coupling between the scalar-meson and the baryon fields which they later adjust to reproduce the experimental conditions at saturation. Their results for the compression modulus,  $\kappa = 224$  MeV, and effective mass,  $M^* = 797$  MeV, compare very well with Skyrme-type calculations [8].

Since it is desirable to have models that, at the mean-field level, provide reasonable nuclear matter results, the original ZM model and its two variations (to which we shall refer hereafter as ZM2 and ZM3) described in the appendix of the original paper of Zimanyi and Moszkowski [6], have deserved some recent attention. Particularly, Koepf, Sharma and Ring [9] (KSR) have performed nuclear-matter and finite-nuclei calculations and compared the ZM model against i) the linear  $\sigma - \omega$  model and, ii) models with non-linear scalar couplings of phenomenological origin. One of their findings was that the ZM model, when used to calculate the energy spectrum of  $^{208}\text{Pb}$ , gives a spin-orbit splitting

that compares poorly with the data. It is well known that the splitting of the energy levels due to the spin-orbit interaction is very sensitive to the difference  $\lambda=V - S$  between the vector,  $V$ , and the scalar,  $S$ , potentials. For the ZM model one gets  $\lambda=223$  MeV, which is short of the 785 MeV of the successful (in this regard) Walecka model. A simplified summary of KSR's results also indicates that: 1) The (non)linear  $\sigma - \omega$  model predicts a (good)reasonable spin-orbit splitting, a (soft)stiff equation of state and a (good)small effective nucleon mass; 2) The ZM model predicts a soft equation of state, a reasonable effective nucleon mass and a poor spin-orbit splitting for finite nuclei. To this list we may add [10,11] that the relativistic content of the various models, as given by the ratio of scalar to baryon densities, differs also being the linear and non-linear  $\sigma - \omega$  models more relativistic than the usual ZM.

At this point it is clear that fixing the spin-orbit problem in the ZM model would make it similar in results to the non-linear  $\sigma - \omega$  model but with the additional bonus of having to fit two parameters instead of four. The modified ZM models, ZM2 and ZM3, aim at this. All three models come about in the following way. In the standard ZM model the non-linear effective scalar factor  $1/m^*=1 + g_\sigma\sigma/M$ , whose meaning will become clear below, multiplies the nucleon derivative and the nucleon-vector coupling terms. When its two free parameters are fitted to the nuclear-matter baryon density,  $\rho_0=0.148 \text{ fm}^{-3}$ , and energy density per nucleon at saturation,  $E_b=-15.75$  MeV, one obtains the results shown in the first row of Table I. If we now let  $1/m^*$  to act upon the nucleon derivative and all terms involving the vector field we end up with the ZM2 version of the ZM model, whose predictions are shown in the second row of the table. The compressibility is slightly lower and the difference between the vector and scalar potentials has increased to 278 MeV [11]. Finally, the ZM3 version of the model is obtained by allowing  $1/m^*$  to act just on the nucleon derivative term. With this change one obtains the results displayed in the third row of the table; the compressibility diminishes again and  $\lambda$  reaches 471 MeV [11]. It is

worth calling the attention to the fact that the particular non-linear couplings used in these models change the traditional conception whereby to a lower value of  $m^* = M^*/M$  should correspond a higher compressibility  $\kappa$ . Particularly, the ZM3 field equations couple the non-linear scalar field to the vector field and this new source is responsible for the  $m^*=0.72$  and  $\kappa=156$  MeV, of the table. In the phenomenological non-linear scalar-coupling model of Feldmeir and Lindner [12] (hiperbolic ansatz), for example, the price to pay for the reduced effective mass,  $m^* = 0.71$ , is an enhanced compressibility,  $\kappa = 410$  MeV.

If we assume that the difference  $\lambda$  between the scalar and the vector potentials is a good indicator of the strength of the spin-orbit splitting in finite nuclei, it is clear from Table I that ZM3 offers the closest approach of the three to the non-linear  $\sigma - \omega$  model. In this situation it is relevant to study the model predictions for a number of properties of finite nuclei for which there exist experimental data. In this work we apply the ZM3 model to the study of the energy spectrum and ground-state properties of  $^{16}\text{O}$ ,  $^{40}\text{Ca}$ ,  $^{48}\text{Ca}$ ,  $^{90}\text{Zr}$  and  $^{208}\text{Pb}$ . We calculate energy levels, charge *r.m.s* radius and nucleon density distributions and compare the results obtained with the predictions of the standard ZM model and with the experimental data in order to extract conclusions.

In the next section we introduce the ZM and ZM3 models and give the necessary detail to understand the origin of the results we obtain. These are presented in the last section where we also draw some conclusions.

## II. THE MODEL

The ZM and ZM3 models of interest for this work can be derived from the Lagrangean

$$\begin{aligned} \mathcal{L} = & \sum_{a=1}^A \bar{\psi}_a \left\{ \gamma_\mu \left[ \left( i\partial^\mu - e \frac{(1 + \tau_3)}{2} A^\mu \right) - g_\omega^* \omega^\mu - \frac{g_\rho^*}{2} \tau_3 \rho^\mu \right] - (M - g_\sigma^* \sigma) \right\} \psi_a \quad (1) \\ & + \frac{1}{2} \left( \partial_\mu \sigma \partial^\mu \sigma - m_\sigma^2 \sigma^2 \right) - \frac{1}{4} \left( \partial_\mu \omega_\nu - \partial_\nu \omega_\mu \right)^2 + \frac{1}{2} m_\omega^2 \omega_\mu \omega^\mu \\ & - \frac{1}{4} \left( \partial_\mu \rho_\nu - \partial_\nu \rho_\mu \right)^2 + \frac{1}{2} m_\rho^2 \rho_\mu \rho^\mu - \frac{1}{4} \left( \partial_\mu A_\nu - \partial_\nu A_\mu \right)^2 , \end{aligned}$$

where the effective coupling constants are given in each model according to

Model	$g_\sigma^*$	$g_{\omega,\rho}^*$
ZM	$m^* g_\sigma$	$g_{\omega,\rho}$
ZM3	$m^* g_\sigma$	$m^* g_{\omega,\rho}$

where we define

$$m^* = \left(1 + \frac{g_\sigma \sigma}{M}\right)^{-1}.$$

In equation (1) the nucleon field,  $\psi$ , couples to the scalar-isoscalar meson field,  $\sigma$ , and the vector-isoscalar meson field,  $\omega_\mu$ . A third isovector meson field,  $\rho_\mu$ , (neutral component) is included to account for the asymmetry between protons and neutrons. The  $\rho_\mu$  and the electromagnetic field  $A_\mu$  both couple to the baryon field.

The Euler-Lagrange equations of motion using the Lagrangean (1) give the following equations for the fields,

$$\left\{ \gamma_\mu \left[ \left( i\partial^\mu - e \frac{(1 + \tau_3)}{2} A^\mu \right) - g_\omega^* \omega^\mu - \frac{g_\rho^*}{2} \tau_3 \rho^\mu \right] - (M - g_\sigma^* \sigma) \right\} \psi_a = 0, \quad (2)$$

$$\partial_\mu \omega^{\mu\nu} + m_\omega^2 \omega^\nu = g_\omega^* \sum_{a=1}^A \bar{\psi}_a \gamma^\nu \psi_a, \quad (3)$$

$$\partial_\mu \rho^{\mu\nu} + m_\rho^2 \rho^\nu = \frac{g_\rho^*}{2} \sum_{a=1}^A \bar{\psi}_a \gamma^\nu \tau_3 \psi_a, \quad (4)$$

$$\partial_\mu A^{\mu\nu} = \frac{e}{2} \sum_{a=1}^A \bar{\psi}_a \gamma^\nu (1 + \tau_3) \psi_a, \quad (5)$$

$$\partial_\mu \partial^\mu \sigma + m_\sigma^2 \sigma = m^{*2} g_\sigma \sum_{a=1}^A \bar{\psi}_a \psi_a - \sum_{a=1}^A \left( \frac{\partial g_\omega^*}{\partial \sigma} \bar{\psi}_a \gamma_\mu \psi_a \omega^\mu + \frac{1}{2} \frac{\partial g_\rho^*}{\partial \sigma} \bar{\psi}_a \gamma_\mu \tau_3 \psi_a \rho^\mu \right). \quad (6)$$

In the mean-field approximation all baryon currents are replaced by their ground-state expectation values. In a system with spherical symmetry the mean value of the spatial components of the vector-meson fields vanish, resulting in the following mean-field equations,

$$\left\{ \gamma_{\mu} i \partial^{\mu} - \gamma_0 \left[ e \frac{(1 + \tau_3)}{2} A^0 - g_{\omega}^* \omega^0 - \frac{g_{\rho}^*}{2} \tau_3 \rho^0 \right] - (M - g_{\sigma}^* \sigma) \right\} \psi_a = 0, \quad (7)$$

$$-\nabla^2 \omega^0 + m_{\omega}^2 \omega^0 = g_{\omega}^* \sum_{a=1}^A \psi_a^{\dagger} \psi_a \equiv g_{\omega}^* \rho_b = g_{\omega}^* (\rho_p + \rho_n), \quad (8)$$

$$-\nabla^2 \rho^0 + m_{\rho}^2 \rho^0 = \frac{g_{\rho}^*}{2} \sum_{a=1}^A \psi_a^{\dagger} \tau_3 \psi_a \equiv g_{\rho}^* \rho_3 = g_{\rho}^* (\rho_p - \rho_n), \quad (9)$$

$$-\nabla^2 A^0 = \frac{e}{2} \sum_{a=1}^A \psi_a^{\dagger} (1 + \tau_3) \psi_a \equiv e \rho_p, \quad (10)$$

$$\begin{aligned} -\nabla^2 \sigma + m_{\sigma}^2 \sigma &= m^{*2} g_{\sigma} \sum_{a=1}^A \bar{\psi}_a \psi_a - \sum_{a=1}^A \left( \frac{\partial g_{\omega}^*}{\partial \sigma} \psi_a^{\dagger} \psi_a \omega^0 + \frac{1}{2} \frac{\partial g_{\rho}^*}{\partial \sigma} \psi_a^{\dagger} \tau_3 \psi_a \rho^0 \right), \quad (11) \\ &\equiv m^{*2} g_{\sigma} \rho_s - \frac{\partial g_{\omega}^*}{\partial \sigma} \rho_b \omega^0 - \frac{\partial g_{\rho}^*}{\partial \sigma} \rho_3 \rho^0. \end{aligned}$$

Equations (7) to (11) are a set of coupled non-linear differential equations which may be solved by iteration. For a given set of initial meson potentials, the Dirac equation (7) is solved. Once the baryon wave functions are determined the source terms for Eqs. (8)-(11) are evaluated and new meson fields are obtained. The procedure is iterated until self-consistency is achieved.

The coupling constants  $g_{\sigma}$  and  $g_{\omega}$  are chosen to reproduce the saturation baryon density in symmetric nuclear matter,  $\rho_0=0.148 \text{ fm}^{-3}$ , and the energy density per nucleon at saturation,  $E/A=-15.75 \text{ MeV}$ . The third coupling constant,  $g_{\rho}$ , is obtained by fitting the bulk symmetry energy in nuclear matter given by the expression

$$a_4 = \frac{g_{\rho}^2}{8m_{\rho}^2} \left( \frac{g_{\rho}^*}{g_{\rho}} \right) \rho_0 + \frac{k_F^2}{6E_F^*} \quad (12)$$

to  $a_4=32.5 \text{ MeV}$  at  $\rho=\rho_0$ . We have used

$$\rho_0 = \frac{2}{3\pi^2} k_F^3$$

and

$$E_F^* = \sqrt{k_F^2 + m^{*2} M^2}.$$

The coupling constants and masses used in the calculations are given in Table II.

### III. RESULTS

Results of the present calculation for the single particle energy levels in  $^{16}\text{O}$ ,  $^{40}\text{Ca}$ ,  $^{48}\text{Ca}$ ,  $^{90}\text{Zr}$ , and  $^{208}\text{Pb}$  are shown in Tables III to V. Through the tables a good overall agreement is obtained, i) between the two models and, ii) with the experimental data. Nonetheless, the ZM3 model fares better than ZM in reproducing the observed spin-orbit splittings. This is due to the difference in the way that the scalar and vector mesonic fields couple to each other —via non-linear effective coupling constants— in each model. This difference is better illustrated in figures 1 to 4 where the “central potential”,  $V_0$ , and the “reduced spin-orbit term”,  $V_{ls}$ , are depicted as functions of the radial distance,  $r$ , for oxygen and lead. We have defined the central potential to be

$$V_0 = V + S \tag{13}$$

with

$$V = g_\omega^* \omega_0$$

and

$$S = -g_\sigma^* \sigma.$$

The reduced spin-orbit term, on the other hand, is given by the expression,

$$V_{ls} = \frac{V' - S'}{2m_s r}, \tag{14}$$

with  $m_s = M - 0.5*(V - S)$  and with the primes denoting partial derivatives with respect to  $r$ . Though the choice of mass in the denominator of Eq. (14) could be opened to some debate, the figures are intended to compare strengths in both models and not to draw absolute conclusions.

Figures 1 and 3 illustrate the origin of the behaviour of both models. ZM is shallower in the center and raises more steeply on the surface than ZM3; this holds true both in



oxygen and in lead. The resulting spin-orbit potential (figures 2 and 4) is, thus, deeper at the surface in ZM3 than in ZM. To estimate the magnitude of this difference we calculated the ratio expected for the spin-orbit splittings in ZM3 and ZM, using the parameters from the fit to nuclear matter of Table I. The result

$$\frac{V_{ls}^{ZM3}}{V_{ls}^{ZM}} \propto \frac{(V - S)^{ZM3} m_{ZM}^*}{(V - S)^{ZM} m_{ZM3}^*} \approx 2.5$$

agrees nicely with the ratios extracted from the levels in tables III-V.

It is worth noticing that our calculated spectra for the ZM model, differ from those presented by KSR in Ref. [9] for the same model. We have traced the origin of this discrepancy to the symmetry energy  $a_4$  used to fit the  $\rho$ -meson coupling constant. Figure 5 illustrates the effect that a decreasing  $a_4$  has on the energy of a few selected single particle orbits in  $^{208}\text{Pb}$ . The shift in energy due to the presence of the  $\rho$ -meson may be as large as 5 MeV depending on the choice of  $a_4$  (the arrow indicates the value used in the calculations shown here,  $a_4 = 32.5$  MeV). The spectrum of  $^{208}\text{Pb}$  calculated with a vanishing  $g_\rho$  agrees with the results of KSR. Notice also that the splittings amongst spin-orbit partners are insensitive to  $g_\rho$  since changes in  $a_4$  shift the levels globally.

At this point one of our conclusions is that, as demonstrated in [9], the ZM model does not do well in reproducing the energy splittings due to the spin-orbit interaction. However, the overall spectrum turns out to be satisfactory. In this sense the isovector meson plays in ZM the same important role, for asymmetric nuclei, that has been shown to play in the non-linear Walecka model [13].

Table VI shows the results obtained for some of the static ground-state properties of the same nuclei as above. One feature to point out is that, systematically, ZM3 predicts a *r.m.s.* value for the charge radius that is larger than the one calculated with the ZM model. This is due to the slightly smaller binding of the protons in this model that produces a longer tail in the charge distribution, as shown in Figs. 6 and 7. The baryon density extends also farther in ZM3 as can be appreciated from Figs. 8 and 9. The baryon

distribution at the surface indicates that edge effects are more important in ZM3 than in the ZM model, something that agrees with our discussion of the spin-orbit splittings in the previous paragraphs.

Summarizing, we have applied the ZM3 model to the study of the energy spectrum and ground-state properties of  $^{16}\text{O}$ ,  $^{40}\text{Ca}$ ,  $^{48}\text{Ca}$ ,  $^{90}\text{Zr}$  and  $^{208}\text{Pb}$ . The interest in this model, and the standard ZM, resides in their ability to describe nuclear matter at saturation with two free parameters. For finite nuclei, we have shown that ZM3 gives a reasonable description of nuclear spectra and improves upon ZM regarding the energy splitting of levels due to the spin-orbit interaction. The results of the calculations described here were compared with those obtained using the standard ZM model and with the experimental data. It is our conclusion that models of this kind, with derivative couplings involving the scalar and the vector fields, offer a valid framework to pursue calculations where the requirement of simultaneous reasonable values for the nuclear compressibility and the spin-orbit splitting cannot be side-stepped.

### **Acknowledgements**

One of the authors (MC) would like to express his thanks to the Conselho Nacional de Desenvolvimento Científico e Tecnológico (CNPq) and to the Departamento de Física Nuclear e Altas Energias (DNE-CBPF) Brazil, for their financial support. AG is a fellow of the the CONICET, Argentina.

## REFERENCES

- [1] J. D. Walecka, Ann. Phys. **83**, 491 (1974); B. D. Serot and J. D. Walecka, Advances in Nuclear Physics Vol. 16, (Plenum, New York, 1986), pp. 1–327; R. J. Furnstahl and B. D. Serot, Phys. Rev. **C41**, 262 (1990).
- [2] G. E. Brown and E. Osnes, Phys. Lett. **B 159**, 223 (1985).
- [3] G. Co´ and J. Speth, Phys. Rev. Lett. **57**, 547 (1986). Comment on preceding paper: A. van der Woude, W. T. A. Borghols, S. Brandenburg, M. M. Sharma and M. N. Harakeh, Phys. Rev. Lett. **58**, 2383 (1987). Response to the comment: G. Co´ and J. Speth, *ibid* **58**, 2384 (1987).
- [4] J. Boguta and A. R. Bodmer, Nucl. Phys. **A292**, 414 (1977).
- [5] B. M. Waldhauser, J. A. Maruhn, H. Stöcker and W. Greiner, Phys. Rev. **C38**, 1003 (1988);
- [6] J. Zimanyi and S. A. Moszkowski, Phys. Rev. **C42**, 1416 (1990).
- [7] E. K. Heide and S. Rudaz, Phys. Lett **B262**, 375 (1991).
- [8] J. Zimanyi *et al*, Nucl. Phys. **A484**, 647 (1988).
- [9] W. Koepf, M. M. Sharma and P. Ring, Nucl. Phys. **A533**, 95 (1991).
- [10] A. Delfino, M. Chiapparini, M. Malheiro, L. V. Belvedere, and A. O. Gattone, Zeit. für Phys. **A** (in press).
- [11] A. Delfino, C. T. Coelho and M. Malheiro, Phys. Lett. **B345**, 361 (1995); Phys. Rev. **C51**, 2188 (1995).
- [12] H. Feldmeier and J. Lindner, Z. Phys. **A341**, 95 (1991).
- [13] M. M. Sharma, S. A. Moszkowski and P. Ring, Phys. Rev. **C44**, 2493 (1991).

## TABLES

TABLE I. Nuclear matter results in the three Zimanyi-Moskowszki models. The compressibility  $\kappa$ , the scalar potential  $S$ , and the vector potential  $V$ , are in MeV. The effective mass is in units of the bare mass.

Model	$\kappa$	S	V	$m^*$
ZM	225.	-141.	82.5	0.85
ZM2	198.	-168.	110.7	0.82
ZM3	156.	-267.	204.7	0.72

TABLE II. Parameters used in the calculation.

Model	$m_N$	$m_\sigma$	$m_\omega$	$m_\rho$	$g_\sigma^2$	$g_\omega^2$	$g_\rho^2$
ZM	938.27	520	783	770	55.540	44.207	79.605
ZM3	938.27	520	783	770	135.30	211.21	137.74

TABLE III. Single-particle energy levels (in MeV) calculated in the Zimanyi-Moszkowski model (ZM) and in the ZM3 version. Where available the experimental energies are also quoted. Numbers between brackets correspond to protons, others to neutrons.

Nucl.	Levels	ZM		ZM3		Exp.	
$^{16}\text{O}$	$1s_{1/2}$	35.4	(31.2)	36.2	(32.1)	47.0	(40±8)
	$1p_{3/2}$	19.6	(15.6)	19.4	(15.6)	21.8	(18.4)
	$1p_{1/2}$	18.2	(14.2)	16.5	(12.7)	15.7	(12.1)
$^{40}\text{Ca}$	$1s_{1/2}$	43.3	(35.1)	46.7	(38.7)		(50±10)
	$1p_{3/2}$	32.4	(24.5)	33.6	(25.9)		(34±6)
	$1p_{1/2}$	31.6	(23.7)	31.9	(24.2)		(34±6)
	$1d_{5/2}$	20.2	(12.6)	20.4	(13.0)	21.9	(15.5)
	$1d_{3/2}$	18.7	(11.2)	17.3	(9.97)	15.6	(8.3)
	$2s_{1/2}$	15.9	(8.33)	16.9	(9.52)	18.2	(10.9)
$^{48}\text{Ca}$	$1s_{1/2}$	41.8	(39.9)	45.7	(43.2)		(55±9)
	$1p_{3/2}$	31.3	(30.7)	33.2	(32.1)		(35±7)
	$1p_{1/2}$	30.8	(30.1)	32.0	(30.7)		(35±7)
	$1d_{5/2}$	19.8	(19.7)	20.4	(20.0)	16.0	(20.0)
	$1d_{3/2}$	18.7	(18.5)	17.9	(17.4)	12.4	(15.3)
	$1f_{7/2}$	7.87		7.94		9.9	
	$2s_{1/2}$	16.7	(14.4)	17.2	(15.4)	12.4	(15.8)

TABLE IV. Same as Table III.

Nucl.	Levels	ZM		ZM3		Exp.
<sup>90</sup> Zr	1s <sub>1/2</sub>	45.9	(37.2)	51.0	(41.6)	(54±8)
	1p <sub>3/2</sub>	38.4	(30.8)	41.6	(33.5)	(43±8)
	1p <sub>1/2</sub>	38.1	(30.5)	40.9	(32.7)	(43±8)
	1d <sub>5/2</sub>	29.7	(22.9)	31.4	(24.3)	(27±8)
	1d <sub>3/2</sub>	29.1	(22.2)	29.9	(22.6)	(27±8)
	1f <sub>7/2</sub>	20.3	(13.8)	20.8	(14.3)	
	1f <sub>5/2</sub>	19.1	(12.6)	18.3	(11.7)	13.5
	1g <sub>9/2</sub>	10.2		10.2		12.0
	2s <sub>1/2</sub>	26.6	(18.2)	28.1	(19.9)	(27±8)
	2p <sub>3/2</sub>	16.0	(7.64)	16.9	(8.88)	13.1
	2p <sub>1/2</sub>	15.6	(7.25)	16.0	(8.01)	12.6

TABLE V. Same as Table III.

Nucl.	Levels	ZM		ZM3		Exp.
<sup>208</sup> Pb	1s <sub>1/2</sub>	45.1	(35.6)	50.6	(40.0)	
	1p <sub>3/2</sub>	41.0	(31.8)	45.3	(35.2)	
	1p <sub>1/2</sub>	40.7	(31.6)	45.1	(34.9)	
	1d <sub>5/2</sub>	35.8	(26.9)	39.0	(29.4)	
	1d <sub>3/2</sub>	35.6	(26.6)	38.4	(28.7)	
	1f <sub>7/2</sub>	29.9	(21.2)	31.9	(22.7)	
	1f <sub>5/2</sub>	29.4	(20.6)	30.9	(21.5)	
	1g <sub>9/2</sub>	23.2	(14.6)	24.3	(15.4)	
	1g <sub>7/2</sub>	22.4	(13.8)	22.6	(13.6)	(11.4)
	1h <sub>11/2</sub>	15.9	(7.41)	16.2	(7.65)	(9.4)
	1h <sub>9/2</sub>	14.8		13.9		10.8
	1I <sub>13/2</sub>	8.18		7.98		9.0
	2s <sub>1/2</sub>	33.2	(23.7)	36.2	(26.1)	
	2p <sub>3/2</sub>	25.8	(16.5)	27.8	(18.1)	
	2p <sub>1/2</sub>	25.6	(16.3)	27.4	(17.6)	
	2d <sub>5/2</sub>	18.1	(8.87)	19.4	(9.92)	(9.7)
	2d <sub>3/2</sub>	17.7	(8.50)	18.5	(9.06)	(8.4)
	2f <sub>7/2</sub>	10.2		11.0		9.7
	2f <sub>5/2</sub>	9.69		9.85		7.9
	3s <sub>1/2</sub>	16.3	(6.75)	17.6	(7.81)	(8.0)
3p <sub>3/2</sub>	7.88		8.83		8.3	
3p <sub>1/2</sub>	7.69		8.38		7.4	

TABLE VI. The binding energy per nucleon  $\varepsilon$  (in MeV), the mean square charge radius  $\langle r^2 \rangle$  (in fm<sup>2</sup>) and, the spin-orbit splitting (for partners where data are available)  $\Delta E_{so}$  (MeV), are shown for the ZM and ZM3 models. The experimental values are shown for reference.

Nucleus	g.s.p.	ZM	ZM3	Exp.
<sup>16</sup> O	$\varepsilon$	-8.40	-7.50	-7.98
	$\langle r^2 \rangle$	2.64	2.78	2.74
	$\Delta E_{so}(1p_{3/2}-1p_{1/2})$	1.4	2.8	6.1
<sup>40</sup> Ca	$\varepsilon$	-9.01	-8.43	-8.55
	$\langle r^2 \rangle$	3.39	3.51	3.48
	$\Delta E_{so}(1d_{5/2}-1d_{3/2})$	1.5	6.1	6.3
<sup>48</sup> Ca	$\varepsilon$	-8.78	-8.30	-8.67
	$\langle r^2 \rangle$	3.47	3.57	3.47
	$\Delta E_{so}(1d_{5/2}-1d_{3/2})$	1.1	2.5	3.6
<sup>90</sup> Zr	$\varepsilon$	-8.80	-8.46	-8.71
	$\langle r^2 \rangle$	4.25	4.35	4.27
	$\Delta E_{so}(2p_{3/2}-2p_{1/2})$	0.4	0.9	0.5
<sup>208</sup> Pb	$\varepsilon$	-7.86	-7.66	-7.87
	$\langle r^2 \rangle$	5.54	5.66	5.50
	$\Delta E_{so}(2f_{7/2}-2f_{5/2})$	0.5	1.15	1.8
	$\Delta E_{so}(3p_{3/2}-3p_{1/2})$	0.19	0.45	0.9



## FIGURES

FIG. 1. The potential  $V_0$  (defined in equation (13) in the text) as a function of the radial distance. The calculation was done in oxygen and the results correspond to the standard Zimanyi-Moszkowski model (ZM) [6] and to the ZM3 model studied in this paper.

FIG. 2. Same as figure 1 but for the  $^{208}\text{Pb}$  nucleus.

FIG. 3. The spin-orbit potential  $V_{ls}$  (defined in equation (14) in the text) as a function of the radial distance. The calculation was done in oxygen and the results correspond to the standard Zimanyi-Moszkowski model (ZM) [6] and to the ZM3 model studied in this paper.

FIG. 4. Same as figure 3 but for the  $^{208}\text{Pb}$  nucleus.

FIG. 5. Valence proton and neutron orbitals in  $^{208}\text{Pb}$  as a function of the asymmetry parameter  $a_4$ . The arrow indicates the value used in the calculations performed in this work.

FIG. 6. The charge density distribution in  $^{16}\text{O}$  as a function of the radial distance. The results correspond to the standard Zimanyi-Moszkowski model (ZM) [6] and to the ZM3 model studied in this paper.

FIG. 7. Same as figure 6 but for the  $^{208}\text{Pb}$  nucleus.

FIG. 8. The baryon density distribution in  $^{16}\text{O}$  as a function of the radial distance. The results correspond to the standard Zimanyi-Moszkowski model (ZM) [6] and to the ZM3 model studied in this paper.

FIG. 9. Same as figure 8 but for the  $^{208}\text{Pb}$  nucleus.

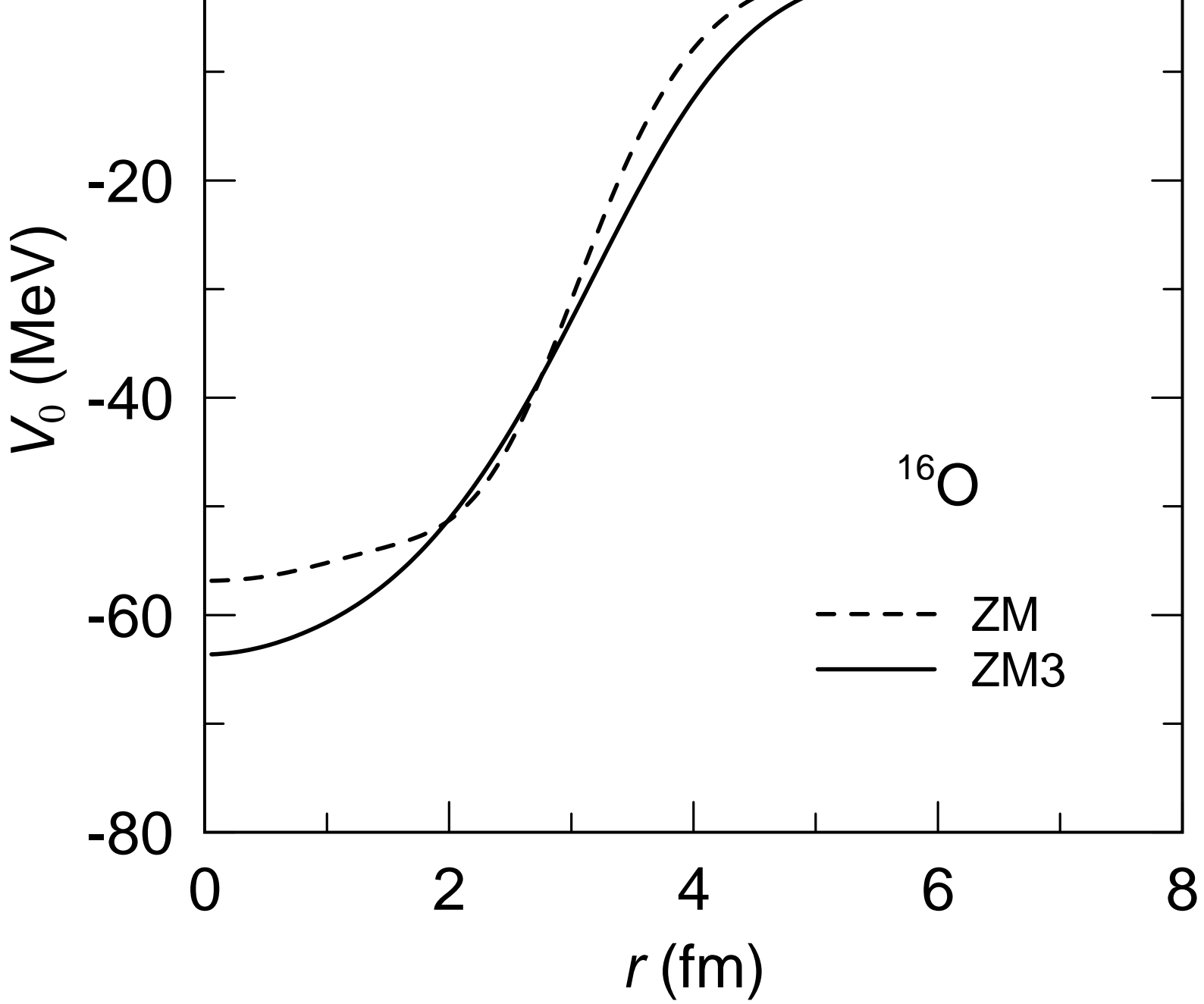


Fig. 1 - M. Chiapparini *et al.*

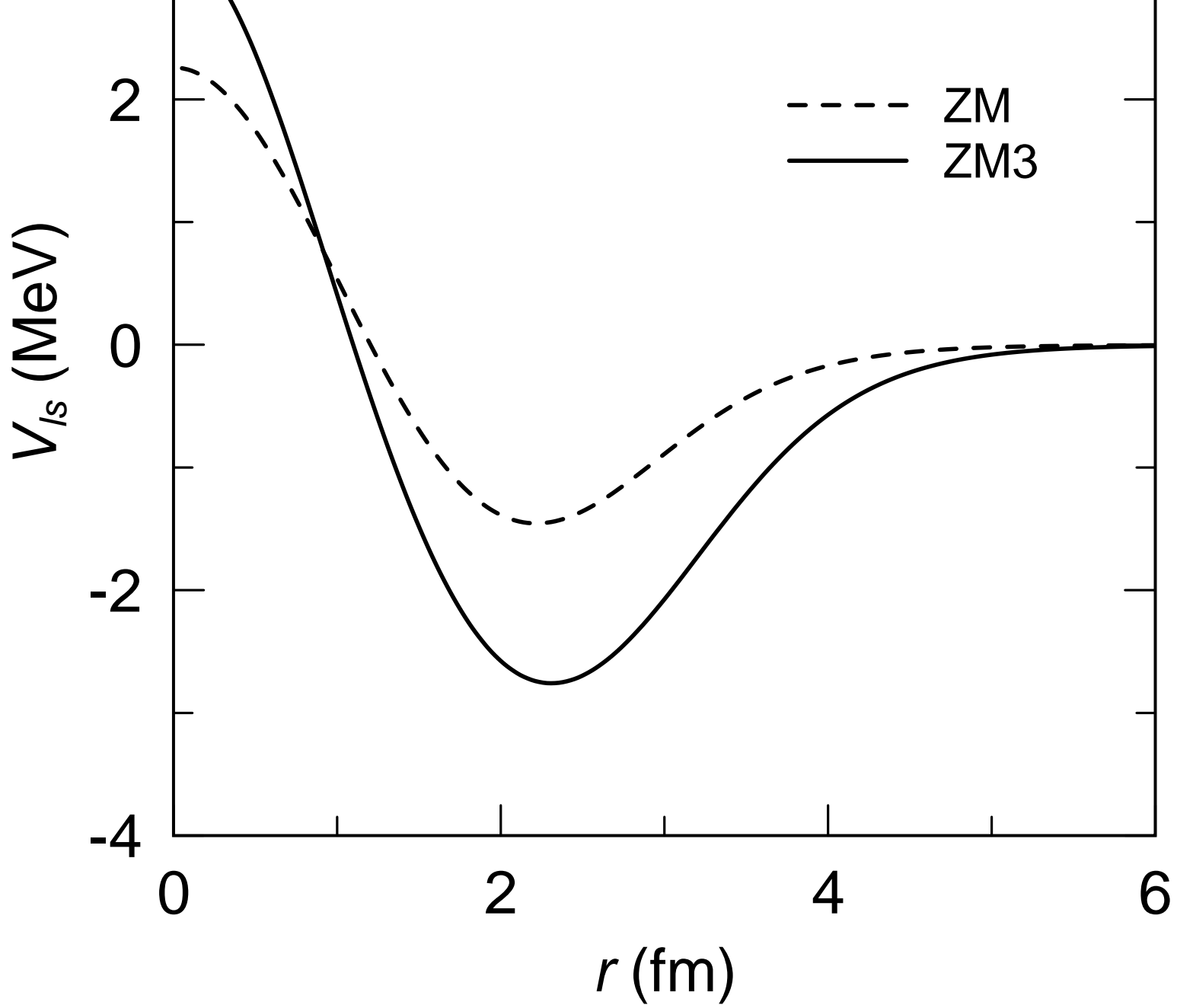


Fig. 2 - M. Chiapparini *et al.*

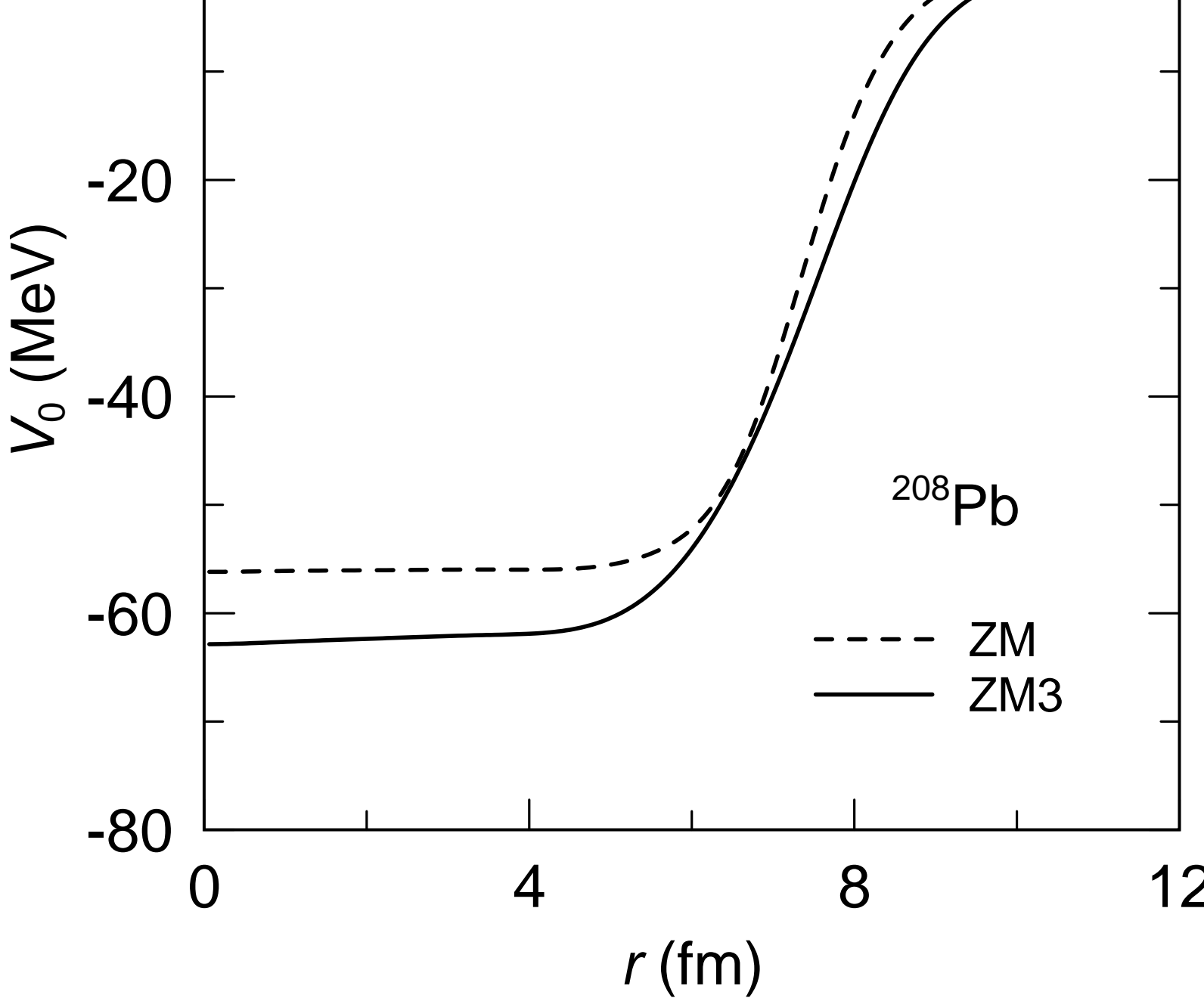


Fig. 3 - M. Chiapparini *et al.*

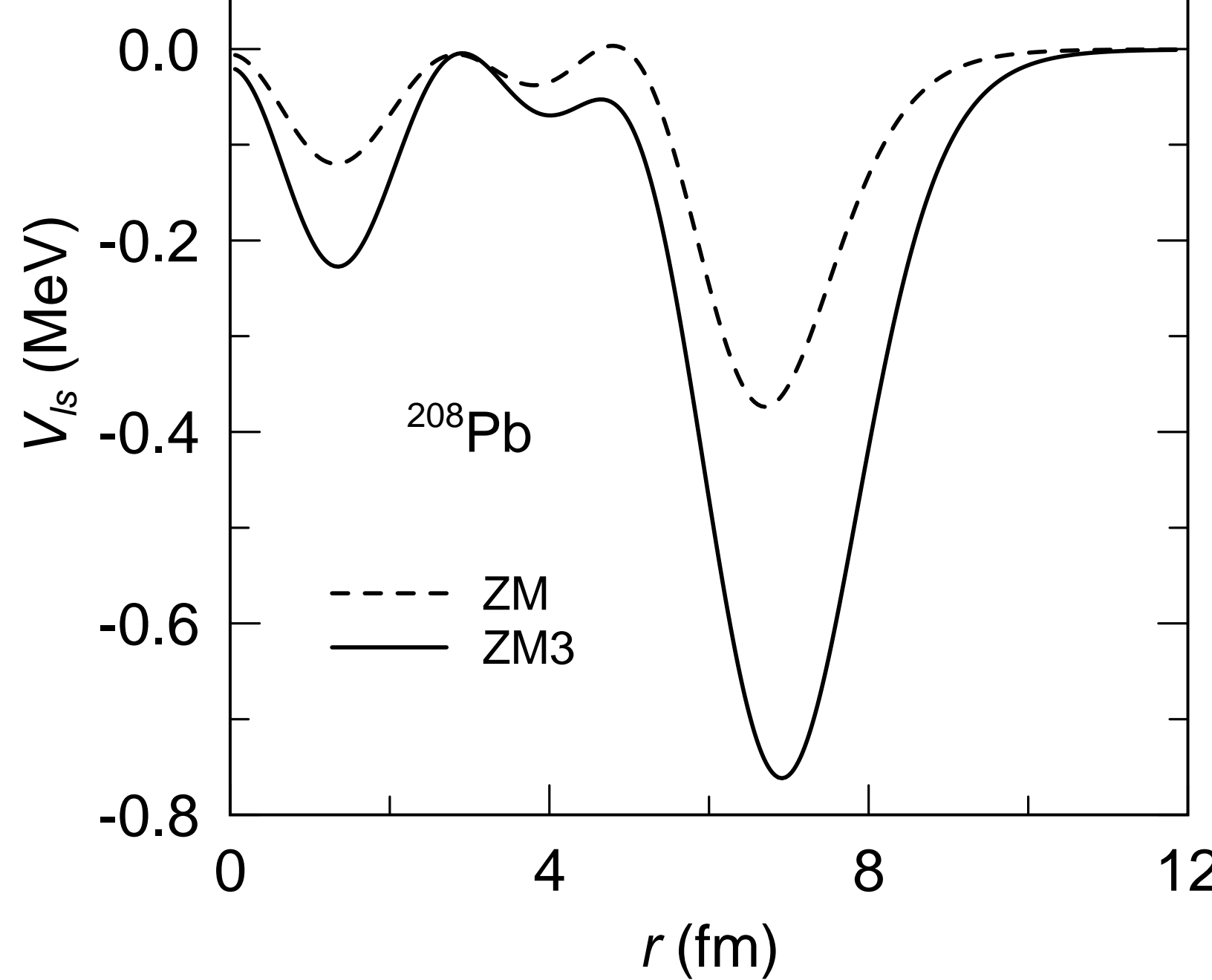


Fig. 4 - M. Chiapparini *et al.*

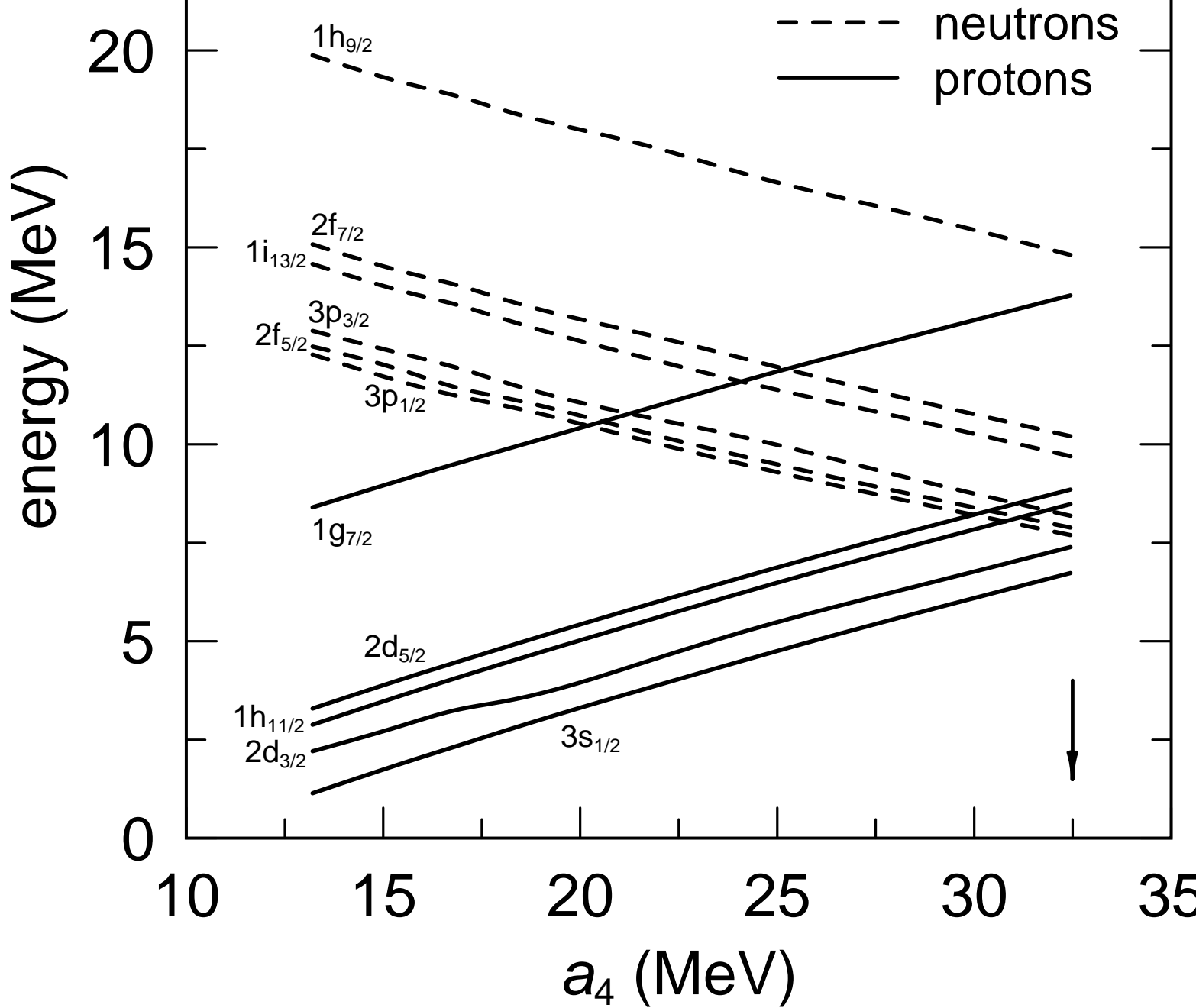


Fig. 5 - M. Chiapparini *et al.*

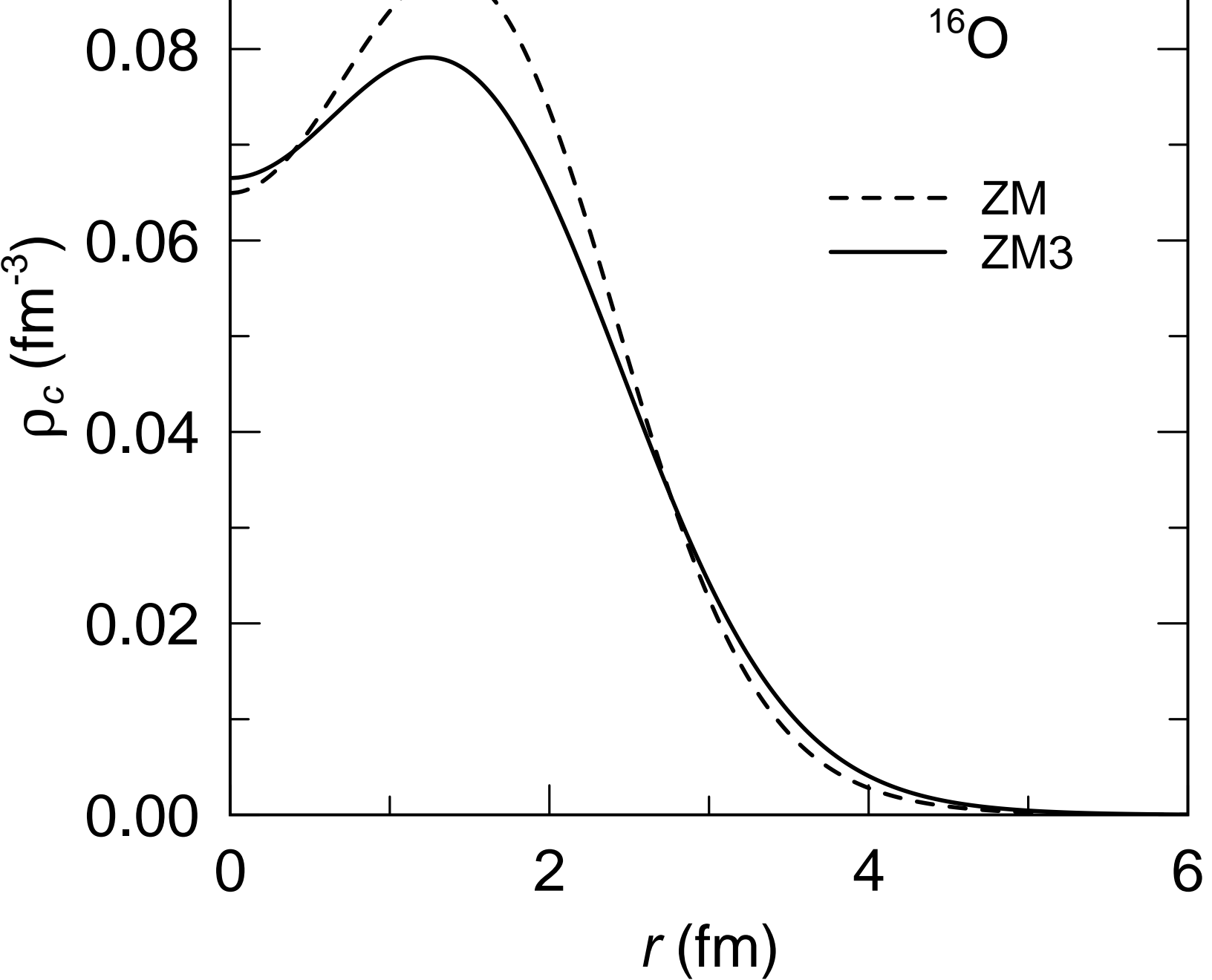


Fig. 6 - M. Chiapparini *et al.*

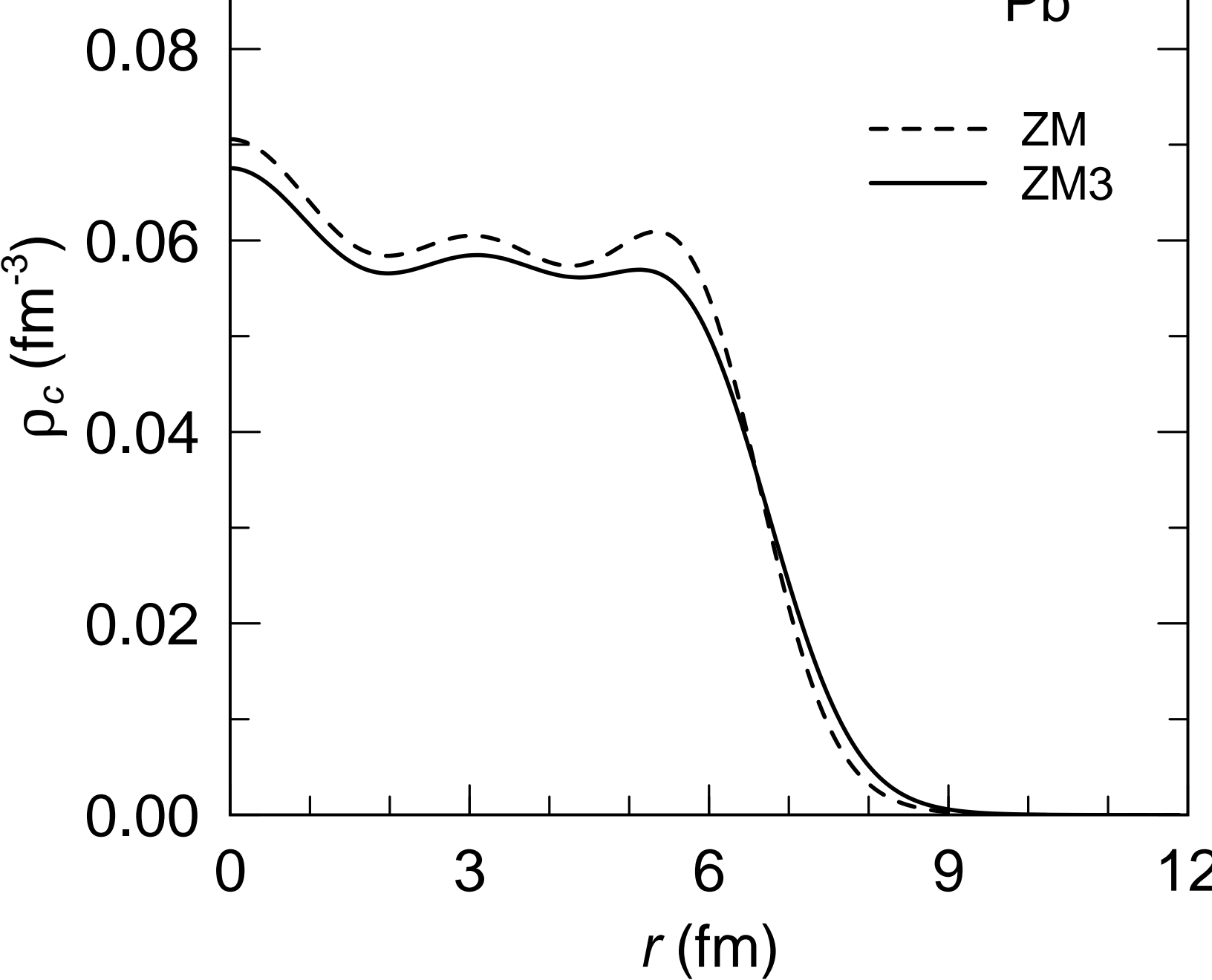


Fig. 7 - M. Chiapparini *et al.*



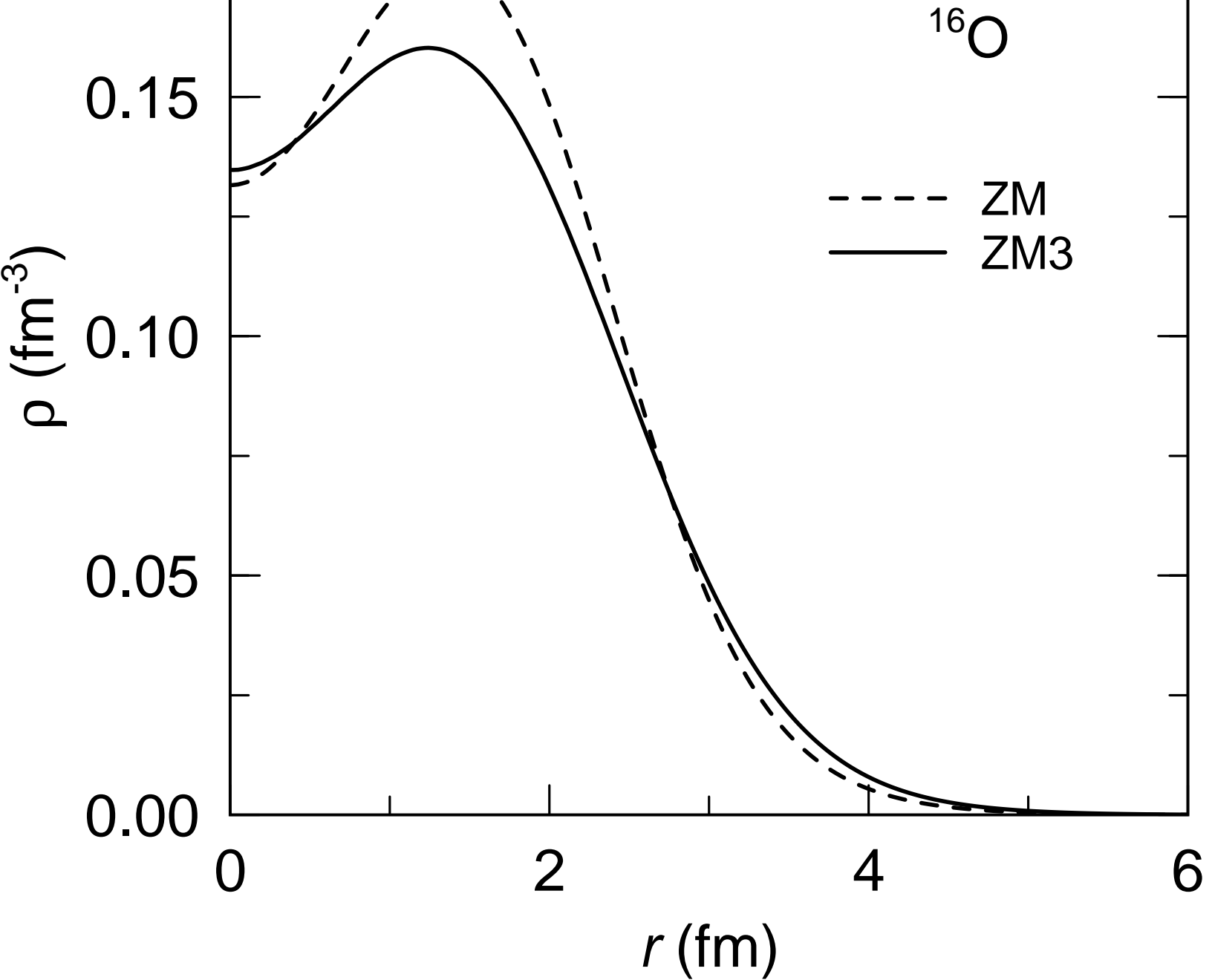


Fig. 8 - M. Chiapparini *et al.*

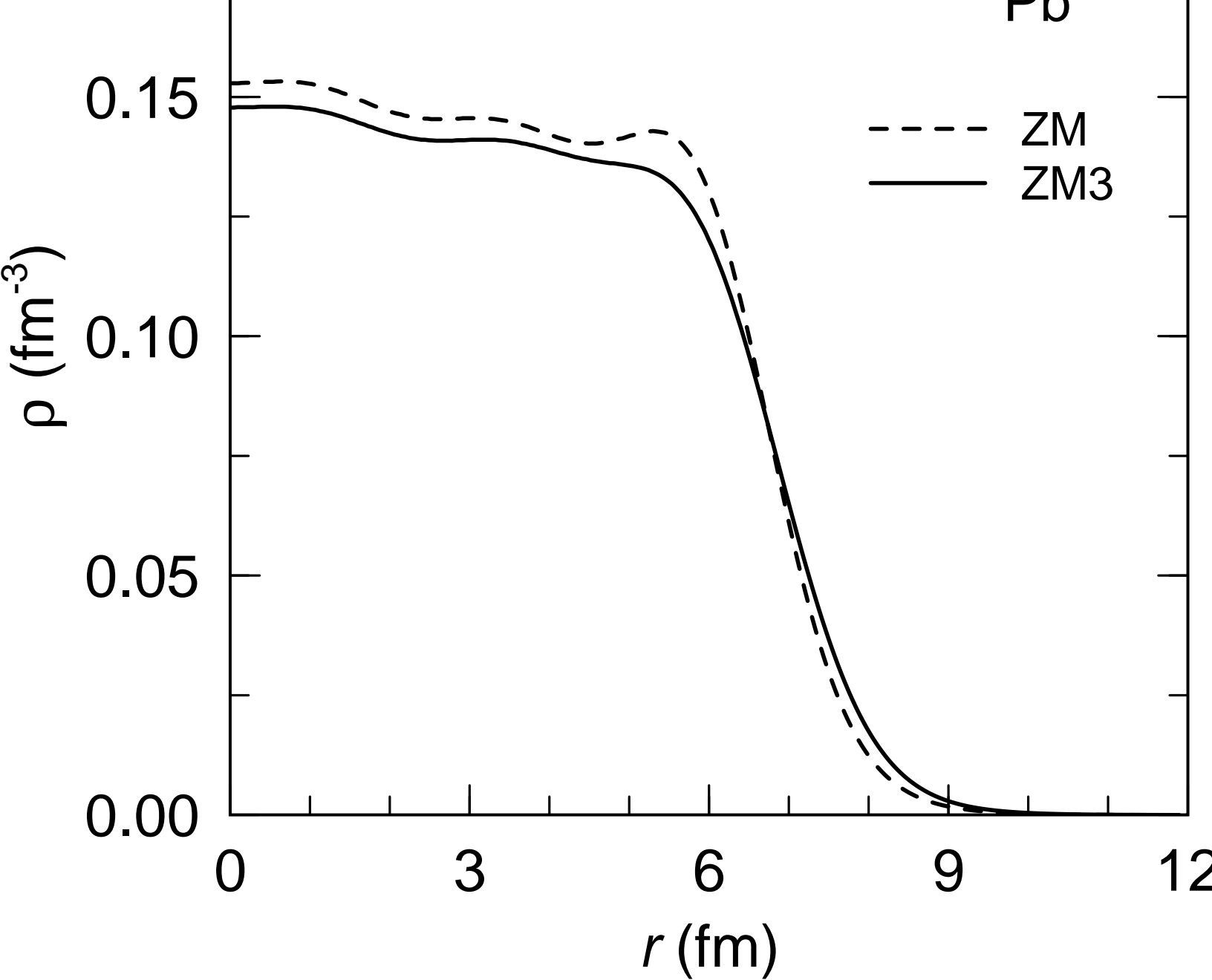


Fig. 9 - M. Chiapparini *et al.*